ELSEVIER

A critical evaluation of near-wall two-equation models against direct numerical simulation data

A. Sarkar and R. M. C. So*
Mechanical and Aerospace Engineering, Arizona State University, Tempe, Arizona

Two-equation turbulence models with near-wall corrections are assessed by applying them to calculate plane Couette flow—a flow case where conventional two-equation models and second-order closures fail to give a correct prediction of the spatial distribution of the turbulent kinetic energy—plane channel flow, and flat plate boundary-layer flow. The predictions of 10 near-wall two-equation models, including the k-τ and k-ω models and 5 recently developed asymptotically consistent near-wall k-ε models, are compared with data obtained from direct numerical simulations at very low Reynolds numbers. It is found that models that are not asymptotically consistent are incapable of predicting the spatial distribution of k correctly in Couette flows. Instead, they give a fairly uniform distribution of k across a substantial portion of the channel. Of all the models evaluated, the asymptotically consistent k-ε models are found to perform the best compard to direct numerical simulation (DNS) data and experimental measurements. Five of the ten models are further validated against DNS data of a backstep flow at low Reynolds number. Similar results as before are obtained. Therefore, the present results lend credence to the hypothesis that an internally consistent and asymptotically correct near-wall model is of crucial importance to the calculations of wall-bounded turbulent flows.

Keywords: near-wall modeling; two-equation models; turbulence modeling

Introduction

Many important scientific and engineering applications involving turbulent flows require the direct integration of the modeled turbulence equations to a solid boundary. Turbulent flows involving boundary-layer separation or complex alterations of the surface transport properties represent but two examples. For these problems, near-wall turbulence modeling plays a crucial role. The predictions of an otherwise sound high Reynolds number turbulence model can be degraded significantly when integrated to a solid boundary without the proper near-wall modifications. Consequently, near-wall turbulence modeling has received considerable attention during the past decade with the bulk of the effort directed towards two-equation and second-order models (Patel et al. 1985; So et al. 1991a: Hanjalic 1994).

The inability to measure turbulence statistics close to a wall reliably has impeded progress in near-wall turbulence modeling. Although advanced optical techniques have been developed recently for the study of near-wall flows, accurate measurements of viscous dissipation is still lacking (Alfredsson et al. 1988; Karlsson and Johansson 1988; Nishino and Kasagi 1989). However, during the past decade, direct numerical simulation (DNS) data have become available for wall-bounded turbulent flows, and these include fully developed plane and curved channel flows (Kim et al. 1987; Mansour et al. 1988; Moser and Moin 1987; Kim 1991), two-dimensional (2-D) flat plate boundary layer (Spalart 1988), fully developed Couette flow (Lee and Kim 1991; Kristoffersen et al. 1993), and backstep flow (Le et al. 1994). These DNS data provide details of the turbulence structure near solid boundaries, which include the fluctuating pressure field and its correlation with the fluctuating velocity field, the viscous dissipation of turbulent kinetic energy, and other higher-order statistics, that far exceed anything that can be obtained from physical experiments. When the DNS data are used in conjunction with the mathematical constraints of asymptotic consistency, a powerful tool is available for the development of improved near-wall turbulence models (Launder 1986; Mansour and Shih 1989; So et al. 1991a; Rodi and Mansour 1993; Hanjalic 1994).

The review article by Patel et al. (1985) summarized the status of near-wall two-equation modeling up to that time. Since then, many more near-wall two-equation models have been proposed using DNS data to help develop more accurate correcting functions to account for near-wall viscous effects. These include k-ε models (Nagano and Hishida 1987; Myong and Kasagi 1990; Deng and Piquet 1991; Karlsson et al. 1991; Michelassi et al.

Address reprint requests to Prof. R. M. C. So, Mechanical Engineering Department, The Hong Kong Polytechnic University, Hung Hom, Kowloon, Hong Kong.

Received 6 February 1995; accepted 6 July 1996

Int. J. Heat and Fluid Flow 18: 197–208, 1997

655 Avenue of the Americas, New York, NY 10010

0142-727X/97/$17.00
PII S0142-727X(96)00088-0

1991; Nagano and Tagawa 1991; So et al. 1991b; Yang and Shih 1993; Zhang et al. 1993; Abe et al. 1994; So et al. 1994), k-τ model (Speziale et al. 1990), and k-ω model (Wilcox 1994). Here k is the turbulent kinetic energy, ε its dissipation rate, τ is a turbulent time scale, and $\omega = \varepsilon/k$ is a specific dissipation rate, after Wilcox (1994). These models were developed making use of DNS data from channel flows only. They were applied to calculate a variety of 2-D flows including compressible flows (Zhang et al. 1993). Good success was reported by the authors. However, none of these models has been systematically evaluated against all three types of basic DNS data; channel flow, Couette flow, and boundary-layer flow. There are subtle differences between these three simple wall shear flows. For example, the k level is relatively high and fairly uniform over a substantial portion of the channel in Couette flow, while this is not true for both channel and boundary-layer flows. On the other hand, there is external flow entrainment in the case of boundary-layer flow but not in Couette and channel flows. However, the calculated von Karman constant κ from the DNS data is constant and is reported to be around 0.40 ± 0.02. A good model should be able to correctly recover the log law, which is valid for all three types of flows, and to accurately reproduce the differences between the three flows over a range of Reynolds numbers.

It has long been argued that conventional high Reynolds number turbulence models are not very suitable for calculating plane Couette flows (Henry and Reynolds 1984). The reason for this can be attributed to the erroneous prediction of the spatial distribution of k across the channel even when anisotropic model as well as second-order and third-order closures are used. Nisizima and Yoshizawa (1987) proposed an anisotropic near-wall k-ε model, and Schneider (1989) suggested a Reynolds-stress model for the calculation of plane Couette flows. Their argument is that the lack of anisotropy in conventional models is the main sources of the incorrect k prediction in plane Couette flow calculations. However, the model of Nisizima and Yoshizawa is not asymptotically consistent in the near-wall region, and their results again show that the calculated value of k, contrary to DNS data and measurements, is still very much in error beyond the near-wall region. Even the higher-order model predictions of Schneider fail to capture the behavior of k correctly. The primary objective of the present paper is to demonstrate that the incorrect prediction of plane Couette flow is due mainly to the inability of the models to mimic the near-wall flow correctly. This incorrect near-wall calculation contributes to a constant k across the channel without predicting a peak near the wall. In other words, if the physical near-wall flow is reproduced correctly by the turbulence model, the rest of the flow could be calculated fairly correctly. Therefore, plane Couette flow is a good test case for any newly developed near-wall two-equation model of turbulence.

The second objective of the present study is to evaluate the performance of the more recently developed near-wall two-equation models against these three basic types of DNS data. Three models that have been evaluated by Patel et al. (1985) as reasonably good are used as baseline models to demonstrate the progress made since then. These are the local models of Jones and Launder (1972) and Launder and Sharma (1974) and the model of Chien (1982). It is impractical to compare all two-equation models; therefore, only three different types of two-equation models—the k-ε, the k-τ, and the k-ω—are evaluated in the present study. As far as the k-τ and k-ω models are concerned, there is only one representative example in each category, and they are given by the models of Speziale et al. (1990) and Wilcox (1994), respectively. Among the k-ε models proposed recently, only four are compared in the present investigation. These include four single-time-scale models, of which three (Myong and Kasagi 1990; Karlsson et al. 1991; So et al. 1991b) are formulated without accounting for the destruction of the dissipation term in the ε-equation and one (Yang and Shih 1993) which includes a proposal to account for the destruction of the dissipation term along the lines suggested by Durbin (1991). The former three models (Myong and Kasagi, 1990; Karlsson et al., 1991; So et al. 1991b) have damping functions proposed for the eddy-viscosity v_t, that depend on $y^+ = yu_\tau/v$, where y is the normal coordinate, $u_\tau = (\tau_o/\rho)^{1/2}$ is the friction velocity, τ_o is the wall shear stress, ν is the kinematic viscosity, and ρ is the fluid density, while the damping functions in the latter model has no y^+ dependence. Among the three former k-ε models, two (Karlsson et al., 1991; So et al. 1991b) are calibrated to give good agreement with boundary-layer flows, while one is derived based on internal flow data. The overall applicability of these models will be best tested by using them to calculate flows other than those reported by the authors. Finally, a new model based on that proposed by So et al. (1991b) is also included in this evaluation of two-equation models. The damping function in this new model does not depend on u_τ. It only depends on a turbulent Reynolds number and a Reynolds number defined with respect to the dissipation velocity and the distance from the wall. Furthermore, the model does not contain a proposal to account for the destruction of the dissipation term. This model, like that of Yang and Shih, makes use of DNS channel flow data to derive the damping function. Details of the development of this last model is given by Sakar (1995). Note that none of these latter k-ε, k-τ, and k-ω models is a local model, because they depend on the normal coordinate.

The modeled equations

Incompressible flows are considered. A Cartesian coordinate system with $y = 0$ at the wall of 2-D Couette, channel, and boundary-layer flows is chosen and fully developed flow is examined. The Reynolds stresses can be expressed in terms of an isotropic eddy-viscosity by invoking gradient transport. Thus simplified, the definitions of the Reynolds stresses and eddy-viscosity can be written for all models examined here as

$$-\overline{u_i u_j} = 2v_t S_{ij} - \frac{2}{3}k\delta_{ij} \tag{1a}$$

$$v_t = C_\mu f_\mu k \Psi \tag{1b}$$

where $S_{ij} = (\partial U_i/\partial x_j + \partial U_j/\partial x_i)/2$ is the mean strain rate, U_i is the ith component of the mean velocity, $\Psi = k/\varepsilon$ for all k-ε models considered, $\Psi = 1/\omega$ for the k-ω model and $\Psi = \tau$ for the k-τ model, C_μ is a model constant, f_μ is a damping function, and the overbar is used to denote time-averaged quantities. The governing mean flow and turbulence equations can then be reduced to

$$\frac{DU}{Dt} = -\frac{1}{\rho}\frac{dP}{dx} + \frac{\partial}{\partial y}\left[(v + v_t)\frac{\partial U}{\partial y}\right] \tag{2}$$

$$\frac{Dk}{Dt} = \frac{\partial}{\partial y}\left[\left(v + \frac{v_t}{\sigma_k}\right)\frac{\partial k}{\partial y}\right] + P_k - \beta^* \varepsilon + \chi \tag{3}$$

$$\frac{D\varepsilon}{Dt} = \frac{\partial}{\partial y}\left[\left(v + \frac{v_t}{\sigma_\varepsilon}\right)\frac{\partial \varepsilon}{\partial y}\right] + C_{\varepsilon 1} f_1 \frac{1}{T_t} P_k - C_{\varepsilon 2} f_2 \frac{\hat{\varepsilon}}{T_t} + \xi \tag{4}$$

where D/Dt is the material derivative. U is the mean axial velocity, P is the mean pressure, $P_k = v_t(\partial U/\partial y)^2$ is the production of k, T_t is a turbulent time scale $\hat{\varepsilon}$ is a reduced ε, t is time, χ and ξ are near-wall correcting functions for the k and ε equations, respectively, f_1 and f_2 are damping functions and σ_k,

σ_ε, $C_{\varepsilon 1}$, and $C_{\varepsilon 2}$ are model constants. For fully developed Couette and channel flows, D/Dt reduces to zero, while for boundary-layer flow D/Dt is given by $(U\partial/\partial x + V\partial/\partial y)$, where V is the mean velocity along the y-direction.

The governing equations for the eight k-ε models, hereafter designated as CH for the Chien (1982) model, JL for the Jones and Launder (1972) model, KTS for the Karlsson et al. (1991) model, LS for the Launder and Sharma (1974) model, MK for the Myong and Kasagi (1990) model, SSA (Sakar 1995) for the new model, SZS for the So et al. (1991b) model, and YS for the Yang and Shih (1993) model, can all be cast into the above form. Therefore, their differences are in the choice for T_t, $\hat{\varepsilon}$ and the specifications for χ and ξ. It should be pointed out that the ε in the ε-equation of the CH, JL, and LS models is a reduced ε where the wall value has been subtracted out. On the other hand, the variable in the ε-equation of all other models is the true dissipation rate. This will become obvious when the boundary condition for ε is specified.

The k-equation used in the k-τ model (Speziale et al. 1990), hereafter designated as SAA, and the k-ω model (Wilcox 1994), hereafter designated as WI, is the same as that used in the k-ε models except for the specification of β^*, which is taken to be 1 for all models other than WI. Wilcox makes use of β^* to enforce the correct near-wall behavior for the variables solved and suggests the following expression for β^*, or

$$\beta^* = \frac{9}{100}\left[\frac{5/18 + (\mathrm{Re}_t/\mathrm{R}_\beta)^4}{1 + (\mathrm{Re}_t/\mathrm{R}_\beta)^2}\right] \tag{5}$$

where R_β is a model constant. The turbulent time scale equation for $\tau = k/\varepsilon$ and the specific dissipation rate equation for $\omega = 1/\tau$ can now be written as

$$\frac{D\tau}{Dt} = \frac{\partial}{\partial y}\left[\left(\upsilon + \frac{\upsilon_t}{\sigma_{\tau 2}}\right)\frac{\partial \tau}{\partial y}\right] + \frac{2}{k}\left(\upsilon + \frac{\upsilon_t}{\sigma_{\tau 1}}\right)\frac{\partial k}{\partial y}\frac{\partial \tau}{\partial y} - \frac{2}{\tau}\left(\upsilon + \frac{\upsilon_t}{\sigma_{t2}}\right)\frac{\partial \tau}{\partial y}\frac{\partial \tau}{\partial y} + (1 - C_{\varepsilon 1})\frac{\tau}{k}P_k + (C_{\varepsilon 2}f_1 f_2 - 1) + \xi \tag{6}$$

$$\frac{D\omega}{Dt} = \frac{\partial}{\partial y}\left[\left(\upsilon + \frac{\upsilon_t}{\sigma_\omega}\right)\frac{\partial \omega}{\partial y}\right] + C_{\omega 1}f_1\frac{\omega}{k}P_k - C_{\omega 2}f_2\omega^2 + \xi \tag{7}$$

The model constants are specified by $\sigma_{\tau 1}$, $\sigma_{\tau 2}$, σ_ω, $C_{\omega 1}$, and $C_{\omega 2}$, while χ and ξ are the near-wall correcting functions. According to Wilcox (1994), the damping function f_μ introduced in the υ_t definition renders the behavior of the k-ω model asymptotically correct in the very near-wall region. This claim is tested in the following comparisons with DNS data.

The differences between these models are summarized in Table 1, while Table 2 lists all the model constants adopted by the authors, and Table 3 tabulates the different damping functions used in the models. In Table 1, the reduced dissipation rates $\tilde{\varepsilon}$ and ε^* used in the SSA and SZS models are given by $\tilde{\varepsilon} = \varepsilon - 2\upsilon(\partial\sqrt{k}/\partial y)^2$ and $\varepsilon^* = \varepsilon - 2\upsilon k/y^2$, respectively. The different Reynolds numbers appearing in Table 3 are defined as $\mathrm{Re}_t = k^2/\upsilon\varepsilon$, $\mathrm{Re}_y = y\sqrt{k}/\upsilon$ and $\mathrm{Re}_\varepsilon = (\upsilon\varepsilon)^{1/4}y/\upsilon$. It can be seen that the only difference between the SSA and SZS models is in the near-wall correcting function, which is a consequence of the completely different damping functions invoked for the eddy-viscosity. The ten models examined assume from one damping function, such as the SSA, SZS, and YS models, to three damping functions, such as the SAA model. The k-ε models are selected for their increasing ability to mimic near-wall flow, with the JL model being the least asymptotically consistent. If the hypothesis that near-wall asymptotic consistency is very important for the correct prediction of wall-bounded flows, particularly Couette flows, is true, the agreement between predictions and data should become better as the model's asymptotic consistency improves, if the same amount of empiricism is introduced into the model. Further comparisons with the calculations of the SAA and WI models are carried out to illustrate the importance of near-wall modeling, irrespective of the type of two-equation models used to predict wall-bounded flows. The SAA and WI models are asymptotically more consistent than the JL model, therefore, they should yield better results than the JL model. If the SAA and WI models do, indeed, give better results, the comparisons would lend further credence to the hypothesis that asymptotic consistency is important in near-wall modeling.

The boundary conditions for U are zero at the wall, or $y = 0$ and $y = 2h$, and $U = U_\infty$ in the free stream. Here, $2h$ is the channel height. As for k, the boundary condition is no-slip at the wall for all the two-equation models examined, while the boundary conditions for ε, τ, and ω are model dependent. Because CH, JL, and LS solve a reduced form of the ε-equation, their boundary conditions are $\varepsilon_w = 0$ at the wall. The boundary condition $\varepsilon_w = [4k_1^+ y_1^{+2} - \varepsilon_1^+]$ is used in the MK model, while $\varepsilon_w = \upsilon(\partial^2 k/\partial y^2)_w$ is specified in the KTS model, and $\varepsilon_w =$

Table 1 Near-wall correcting functions for the near-wall turbulence models tested

Model	χ	T_t	$\hat{\varepsilon}$	ξ
CH	$-2\upsilon k/y^2$	k/ε	ε	$2\upsilon\varepsilon\exp[-y^+/2]/y^2$
JL	$-2\upsilon(\partial\sqrt{k}/\partial y)^2$	k/ε	ε	$2\upsilon\upsilon_t(\partial^2 U/\partial y^2)^2$
KTS	0	k/ε	ε	0
LS	$-2\upsilon(\partial\sqrt{k}/\partial y)^2$	k/ε	ε	$2\upsilon\upsilon_t(\partial^2 U/\partial y^2)^2$
MK	0	k/ε	ε	0
SAA	0	—	—	0
SSA	0	k/ε	$\tilde{\varepsilon}$	$\exp\left[-\left(\frac{\mathrm{Re}_t}{40}\right)^2\right]\left[-0.57\frac{\varepsilon\tilde{\varepsilon}}{k} + 0.5\frac{(\varepsilon^*)^2}{k} - 2.25\frac{\varepsilon}{k}P_k\right]$
SZS	0	k/ε	$\tilde{\varepsilon}$	$\exp\left[-\left(\frac{\mathrm{Re}_t}{64}\right)^2\right]\left[-2.0\frac{\varepsilon\tilde{\varepsilon}}{k} + 1.5\frac{(\varepsilon^*)^2}{k}\right]$
YS	0	$\frac{k}{\varepsilon} + \left(\frac{\nu}{\varepsilon}\right)^{1/2}$	ε	$\nu\nu_t(\partial^2 U/\partial y^2)^2$
WI	0	—	—	0

Table 2 Model constants for the near-wall turbulence models tested

Model	σ_k	σ_ε	$\sigma_{\tau 1}$	$\sigma_{\tau 2}$	σ_ω	$C_{\varepsilon 1}$	$C_{\varepsilon 2}$	$C_{\omega 1}$	$C_{\omega 2}$	C_μ	Other
CH	1.0	1.3	—	—	—	1.35	1.8	—	—	0.090	—
JL	1.0	1.3	—	—	—	1.55	2.0	—	—	0.090	—
KTS	1.0	1.3	—	—	—	1.44	1.92	—	—	0.090	$m=3\times10^{-5}$ $n=2.9$
LS	1.0	1.3	—	—	—	1.44	1.92	—	—	0.090	—
MK	1.4	1.3	—	—	—	1.4	1.8	—	—	0.090	—
SAA	1.36	1.36	1.36	1.36	—	1.44	1.83	—	—	0.090	—
SSA	1.0	1.45	—	—	—	1.5	1.83	—	—	0.096	—
SZS	0.75	1.45	—	—	—	1.5	1.83	—	—	0.096	—
YS	1.0	1.3	—	—	—	1.44	1.92	—	—	0.090	$a_1=1.5\times10^{-4}$ $a_3=5.0\times10^{-7}$ $a_5=1.0\times10^{-10}$
WI	2.0	—	—	—	2.0	—	—	5/9	3/40	1.0	$R_k=6$ $R_\omega=2.7$ $R_\beta=8$ $\alpha_o=0.1$ $\alpha_o^*=C_{\omega 2}/3$

$2\upsilon(\partial\sqrt{k}/\partial y)_w^2$ is assumed in the SSA, SZS, and YS models. The subscripts w and 1 are used to denote the wall and the first grid point, respectively. On the other hand, $\tau_w = 0$ is assumed for the SAA model. Strictly speaking, ω_w is infinite at the wall for the WI model. However, in practice, $\omega_1 = (2u_\tau^2/\upsilon\beta^*)/(y_1^{+2})$ is proposed by Wilcox (1994) based on an asymptotic analysis of the ω-equation. These conditions are summarized in Table 3.

Methods of solution

In the case of channel and Couette flows, a finite volume method is used to discretize the governing equations and a time-marching technique is applied to solve the finite-difference equations. Steady-state solutions are obtained when the calculated flow properties at two consecutive time steps are in agreement to

Table 3 The damping functions assumed for the near-wall turbulence models tested

Model	f_1	f_2	f_μ	Wall BC
CH	1	$1-0.3\exp\left[-\left(\frac{\mathrm{Re}_t}{6}\right)^2\right]$	$1-\exp(-0.0115y^+)$	$\varepsilon_w=0$
JL	1	$1-0.3\exp(-\mathrm{Re}_t^2)$	$\exp\left[-\frac{2.5}{1+\mathrm{Re}_t/50.0}\right]$	$\varepsilon_w=0$
KTS	1	$1-\exp[-0.02\,(y^+)^2]$	$1+\frac{0.39}{y^+}\frac{[1-2.468y^+]}{\exp[-m(y^+)^n]}$	$\varepsilon_w=\nu\left(\frac{\partial^2 k}{\partial y^2}\right)_w$
LS	1	$1.0-0.3\exp(-\mathrm{Re}_t^2)$	$\exp\left[-\frac{3.4}{(1.0+\mathrm{Re}_t/50)^2}\right]$	$\varepsilon_w=0$
MK	1	$\left\{1-\frac{2}{9}\exp\left[-\left(\frac{\mathrm{Re}_t}{6}\right)^2\right]\right\}\times[1-\exp(-y^+/5)]^2$	$\left(1+\frac{3.45}{\sqrt{\mathrm{Re}_t}}\right)\left[1-\exp\left(-\frac{y^+}{70}\right)\right]$	$\varepsilon_w=\left[\frac{4k_1^+}{y_1^{+2}}-\varepsilon_1^+\right]$
SSA	$1-\frac{2}{9}\exp\left(-\frac{\mathrm{Re}_t}{6}\right)^2$	$[1-\exp(-y^+/4.9)]^2$	$\left[1+\frac{3.45}{\sqrt{\mathrm{Re}_t}}\right]\tanh\left(\frac{y^+}{70}\right)$	$\tau_w=0$
SSA	1	1	$(1+3/\mathrm{Re}_t^{3/4})\times[1+80\exp(-\mathrm{Re}_\varepsilon)]\times[1-\exp(-\mathrm{Re}_\varepsilon/43-\mathrm{Re}_\varepsilon^2/330)]^2$	$\varepsilon_w=2\nu\left(\frac{\partial\sqrt{k}}{\partial y}\right)_w^2$
SZS	1	1	$\left[1+\frac{3.45}{\sqrt{\mathrm{Re}_t}}\right]\tanh\left(\frac{y^+}{115}\right)$	$\varepsilon_w=2\nu\left(\frac{\partial\sqrt{k}}{\partial y}\right)_w^2$
YS	1	1	$[1-\exp(-a_1\mathrm{Re}_y-a_3\mathrm{Re}_y^3-a_5\mathrm{Re}_y^5)]^{1/2}$	$\varepsilon_w=2\nu\left(\frac{\partial\sqrt{k}}{\partial y}\right)_w^2$
WI	$\frac{\alpha_0+\mathrm{Re}_t/\mathrm{R}_\omega}{C_\mu f_\mu(1+\mathrm{Re}_t/\mathrm{R}_\omega)}$	1	$\frac{\alpha_0^*+\mathrm{Re}_t/\mathrm{R}_k}{1+\mathrm{Re}_t/\mathrm{R}_k}$	$\omega_1=\frac{(2u_\tau^2)}{\nu\beta^* y_1^{+2}}$

within a specified convergence criterion. All the above equations can be cast into a common form if the terms on the right-hand side, besides the diffusion term, are considered to be source terms. Therefore, the finite-difference equation for $\Phi = U, k, \varepsilon, \tau$, or ω can be written as:

$$\Phi^{n+1} = \Phi^n + \frac{2\Delta t}{(\Delta y_j + \Delta y_{j-1})}(\zeta_{j+1/2} - \zeta_{j-1/2}) + \Delta t A_j \tag{8}$$

where A_j is the source term in the equation and is zero for the U equation, $\Delta y_j = y_{j+1} - y_j$, and $\zeta_{j+1/2}$ and $\zeta_{j-1/2}$ are the gradients of Φ approximated by central differences. The convergence criterion is defined with respect to U and is given by

$$\sigma = \left| \frac{U^{n+1} - U^n}{\Delta t U^n} \right| \tag{9}$$

where $\sigma = 10^{-8}$ is assumed for all calculated cases. When this is satisfied, the k convergence according to an expression similar to Equation 9 is about 10^{-5}.

To use a common numerical algorithm to solve the channel and Couette flows, the following transformation is carried out for the Couette flow. The moving wall velocity of the Couette flow is specified as $2U_w$, therefore, the centerline velocity is U_w. This configuration can be easily transformed to an equivalent one where the top wall velocity is U_w, and the bottom wall velocity is $-U_w$, and the centerline velocity is zero. The calculation can be performed over one half of the channel. In other words, the flow in the half channel is equivalent to a plane Couette flow with moving wall velocity U_w and channel width h. In this new configuration, the coordinate system is attached to the stationary wall where y is equal to zero. The governing equations are normalized by U_w and h before solving, and the Reynolds number $\mathrm{Re} = U_w h/\nu$ is the only dimensionless parameter present. Specifying Re is equivalent to fixing the mass flow rate through the channel, and u_τ becomes a calculated result. Therefore, if the calculated U^+ at the centerline does not agree with data, the error is in the predicted wall shear stress. In the case of channel flow, the equations are normalized by u_τ and h; therefore, $\mathrm{Re}_\tau = u_\tau h/\nu$ appears as the only dimensionless parameter in the equations. The equations are solved by specifying Re_τ or equivalently the pressure gradient. With this formulation, the mass flow rate is not specified, thus error in centerline U^+ reflects an incorrect estimate of the centerline U rather than u_τ. A nonuniform grid is used to carry out the calculations, and for accurate resolution of the near-wall flow, at least five grid points are located within $0 \le y^+ \le 5$ and 25 grid points within $5 \le y^+ \le 50$. Therefore, both the viscous sublayer and the buffer layer are resolved properly. Grid-independent studies have been carried out using LS, MK, SAA, SSA, and YS. The results thus obtained are grid independent where the number of grid points are not less than 60 in the y-direction. As a result, the final choice on the grid is 110 for all models for both the Couette and channel-flow calculations.

On the other hand, the boundary-layer calculations are carried out using the code of Wilcox (1994) and the results are compared at a given $\mathrm{Re}_\theta = U_\infty \theta/\nu$, where θ is the momentum thickness of the boundary layer. This code automatically varies the grid number based on a prescribed tolerance at the edge of the boundary layer. Because a common numerical technique is used to perform calculations in each flow type for all models examined, all model calculations are compared on the same basis. This way, any discrepancies between model predictions would actually reflect the true differences between the performance of the models.

Comparisons with simple flows

Five sets of DNS data are used; these are the Couette flow data of Lee and Kim (1991) and Kristoffersen et al. (1993), the channel flow data of Kim et al. (1987) and Kim (1991), and the boundary-layer data of Spalart (1988). In addition, the calculations are compared with a set of experimental data on boundary-layer flow with detailed near-wall measurements at $\mathrm{Re}_\theta = 2420$ (Karlsson and Johansson 1988). The Couette flows examined have $\mathrm{Re} = 1300$ and 3000, or $\mathrm{Re}_\tau = 85$ and 170, respectively. In these cases, U_w is given, so the calculated u_τ is compared in the form u_τ/U_w, which is given by the authors. On the other hand, the channel flows are calculated by specifying Re_τ. The two cases studied have $\mathrm{Re}_\tau = 180$ and 395. Because u_τ is given in these two cases, the calculated centerline velocity U_c is compared with data. The two boundary-layer flows are evaluated at $\mathrm{Re}_\theta = 1410$ and 2420, respectively. Because θ is specified, only the calculated

Table 4 Comparisons of calculated asymptotes' κ and u_τ with data for Couette flows

Couette flow variable	DNS data	Model calculations									
		CH	JL	KTS	LS	MK	SAA	SSA	SZS	YS	WI
Re=1300											
Re_τ=85											
κ	0.40	0.28	0.45	0.48	0.37	0.33	0.34	0.43	0.32	0.42	0.32
u_τ/U_w	0.033	0.031	0.032	0.032	0.032	0.031	0.031	0.032	0.033	0.032	0.032
a_k	0.12	0.06	0.037	0.074	0.02	0.051	0.163	0.096	0.109	0.178	0.008
$\varepsilon_w/2$	—	0.0	0.0	0.068	0	0.049	0.021	0.093	0.109	0.178	0.0
$a_{uv} \times 10^3$	1.61	0.634	0.868	2.033	0.17	1.067	3.21	1.87	0.867	0.467	0.001
Re=3000											
Re_τ=170											
κ	0.40	0.36	0.44	0.46	0.42	0.37	0.39	0.42	0.39	0.41	0.33
u_τ/U_w	0.029	0.028	0.029	0.029	0.03	0.028	0.028	0.029	0.029	0.029	0.026
a_k	—	0.06	0.04	0.075	0.02	0.051	0.10	0.091	0.109	0.182	0.008
$\varepsilon_w/2$	—	0.0	0.0	0.068	0.0	0.05	0.019	0.093	0.108	0.178	0.0
$a_{uv} \times 10^3$	—	0.64	0.949	1.866	0.19	0.933	1.85	1.80	0.85	0.52	0.001

Table 5 Comparisons of calculated asymptotes' κ and U_c with data for channel flows

Channel flow variable	DNS data	Model calculations									
		CH	JL	KTS	LS	MK	SAA	SSA	SZS	YS	WI
$Re_\tau = 180$											
κ	0.40	0.28	0.44	0.49	0.31	0.32	0.34	0.39	0.32	0.39	0.38
U_c/u_τ	18.20	19.14	18.73	17.37	18.90	18.25	18.26	17.47	17.30	17.47	16.51
a_k	0.080	0.042	0.024	0.051	0.010	0.038	0.056	0.080	0.096	0.150	0.200
$\varepsilon_w/2$	0.083	0.0	0.0	0.060	0.0	0.033	0.013	0.080	0.090	0.148	0.0
$a_{uv} \times 10^3$	0.7	0.48	0.62	0.82	0.071	0.62	1.43	1.3	0.76	0.36	0.003
$Re_\tau = 395$											
κ	0.40	0.31	0.45	0.50	0.34	0.35	0.37	0.41	0.40	0.43	0.37
U_c/u_τ	19.96	20.74	20.15	19.20	20.10	20.09	20.06	19.46	19.32	19.22	18.70
a_k	0.106	0.045	0.032	0.050	0.012	0.042	0.073	0.086	0.100	0.167	0.022
$\varepsilon_w/2$	0.110	0.0	0.0	0.070	0.0	0.040	0.016	0.086	0.100	0.165	0.0
$a_{uv} \times 10^3$	1.1	6.0	0.77	0.82	0.075	0.68	1.87	1.39	0.80	0.39	0.003

skin friction coefficients $C_f = 2\tau_o/\rho U_\infty^2$ are compared. All these values are tabulated in Tables 4–6.

Comparisons are made by plotting the results in the form of $U^+ = U/u_\tau$, $k^+ = k/u_\tau^2$, $-uv^+ = -\overline{uv}/u_\tau^2$ and $\varepsilon^+ = v\varepsilon/u_\tau^4$ *versus* $\ln(y^+)$. Here, u and v are the fluctuating velocity components along the x and y directions, respectively. Detailed comparisons are made with data whenever possible. However, only the comparisons with k^+ and ε^+ are shown here. The calculations of U^+ and $-uv^+$ are not shown because, in general, they are in good agreement with data. The results for the Couette flows are given in Figure 1, those for the channel flows are plotted in Figures 2 and 3 and the boundary-layer flow comparisons are displayed in Figures 4 and 5. In addition, data on f_μ are available from Kim et al. (1987), Kim (1991) and Karlsson and Johansson (1988). The comparisons with these data are shown in Figures 6–8, and the ability of the models to correctly predict κ is also assessed. In determining κ, the following procedure is adopted. The authors' reported κ in each data case is used to determined the range of y^+ where the log-law is applicable. A straight line is drawn through the same range of y^+ in a semilog plot of U^+ to evaluate the slope of the straight line and, hence, κ for each calculated flow case. The κ thus determined is listed in Tables 4–6.

Finally, the near-wall asymptotes of k^+, $-uv^+$, and ε^+ are calculated in order to analyze the asymptotic consistency of the different models. According to Launder (1986) k^+, uv^+, and ε^+ near a wall can be expanded in terms of y^+ as

$$k^+ = a_k y^{+2} + b_k y^{+3} + ,\ldots, \tag{10}$$

$$-uv^+ = a_{uv} y^{+3} + b_{uv} y^{+4} + ,\ldots, \tag{11}$$

$$\varepsilon^+ = 2a_k + 4b_k y^+ + ,\ldots, \tag{12}$$

where a_k, b_k, and a_{uv}, b_{uv} are coefficients in the expansions for k^+ and $-uv^+$, respectively. Therefore, the ratio $k^+/\varepsilon^+ y^{+2}$ is exactly $1/2$ at the wall and serves as a check on the asymptotic consistency of the two-equation models. In view of this, two independent ways of determining a_k are available, one from the slope of the k^+ distribution and another from ε_w^+. If the model is asymptotically consistent, the two values of a_k thus determined are equal. Their difference is an indication of the model's deviation from correct asymptotic behavior. Although CH, JL, and LS solve for the reduced ε with $\varepsilon_w = 0$ at the wall, the true ε can be reconstructed. In the present investigation, this is not carried out. The calculated values of a_k, $\varepsilon_w^+/2$ and a_{uv} are also listed in Table 4–6.

Table 6 Comparisons of calculated asymptotes' κ and C_f with data for boundary-layer flows

Boundary-layer flow variable	DNS and exp. data	Model calculations									
		CH	JL	KTS	LS	MK	SAA	SSA	SZS	YS	WI
$Re_\theta = 1410$											
κ	0.41	0.33	0.54	0.44	0.56	0.39	0.39	0.41	0.34	0.41	0.32
$C_f \times 10^3$	4.1	3.76	3.47	4.2	3.38	4.63	4.64	4.04	4.03	4.09	3.81
a_k	—	0.056	0.045	0.07	0.007	0.178	0.171	0.089	0.105	0.22	0.06
$\varepsilon_w/2$	0.13	0.0	0.0	0.069	0.0	0.165	0.141	0.091	0.106	0.164	0.0
$a_{uv} \times 10^3$	—	0.63	0.45	0.013	0.053	0.017	0.015	1.90	0.70	0.453	0.005
$Re_\theta = 2420$											
κ	0.41	0.33	0.52	0.45	0.46	0.41	0.43	0.42	0.36	0.41	0.31
$C_f \times 10^3$	3.54	3.41	3.33	3.80	3.10	4.13	4.16	3.63	3.62	3.68	3.44
a_k	—	0.056	0.031	0.07	0.010	0.136	0.164	0.091	0.105	0.22	0.05
$\varepsilon_w/2$	0.10	0.0	0.0	0.069	0.0	0.161	0.131	0.092	0.106	0.154	0.0
$a_{uv} \times 10^3$	—	0.63	0.69	0.013	0.068	0.013	0.017	0.90	0.70	0.63	0.008

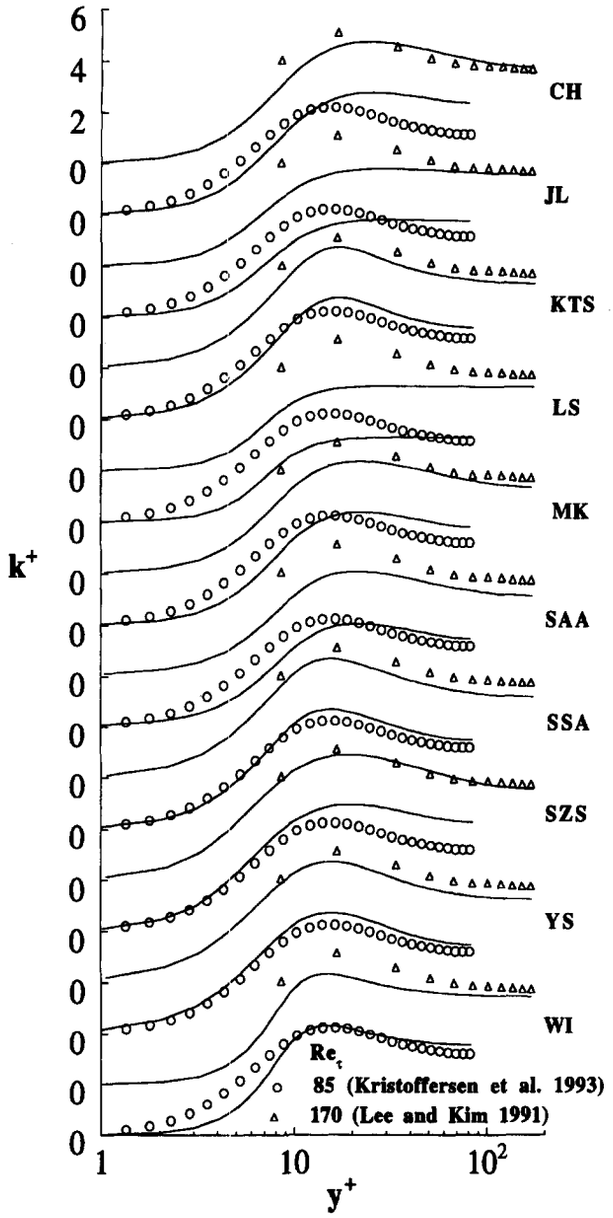

Figure 1 Comparison of calculated k^+ with data for Couette flows

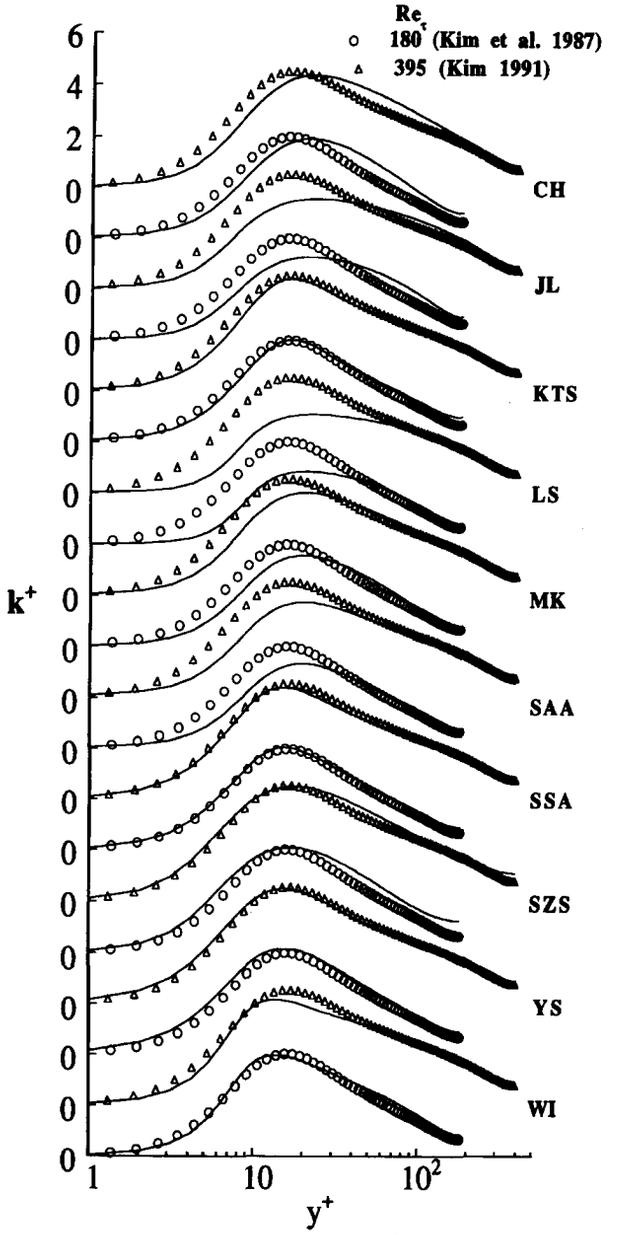

Figure 2 Comparison of calculated k^+ with data for channel flows

From the Couette flow results, it can be seen that SSA and YS yield a fairly accurate prediction of κ, while the worst prediction is given by WI (Table 4). The accuracy in the prediction of u_τ is also compared in Table 4. These results show that the prediction of u_τ by all models is accurate to within 6% of each other. The calculated spatial distributions of k^+ by JL and LS fail to yield the expected behavior characterized by a sharp rise to a maximum near the wall and a gradual drop to a constant value in the central core of the channel (Figure 1). While the performance of JL and LS is worst for the $Re_\tau = 170$ case, CH gives a relatively poorer agreement with data for the $Re_\tau = 85$ case (Figure 1). Other k-ε models, such as CH, KTS, MK, and SZS, give some improvements in the predictions of k^+; however, they are still substantially in error compared to the data. The performance of SAA and WI is not much better compared to these k-ε models. It seems that, with the exceptions of SSA and YS, the model performance is highly dependent on Re. These comparisons show that the correct prediction of the spatial distribution of k^+ in a Couette flow is strongly influenced by the model's ability to reproduce the near-wall flow. This observation is substantiated by the calculated a_k and $\varepsilon_w^+/2$ (Table 4). Although KTS, MK, SSA, SZS, and YS are asymptotically consistent, only SSA and SZS yield values of a_k and $\varepsilon_w^+/2$ approximately equal to those given by DNS data. As for the prediction of a_{uv}, SSA yields a value that agrees to within 20% of the DNS data. Other model calculations are greatly in error.

In the channel flow case, three models yield an overall reasonable prediction of k^+, and they are KTS, SSA, and YS (Figure 2). Other model calculations are either wrong in the inner region, such as those given by JL, LS, MK, and SAA, or near the channel core, such as those predicted by CH and SZS. Predictions of ε^+ are generally in good agreement with data beyond $y^+ = 25$ for all models (Figure 3). The only difference

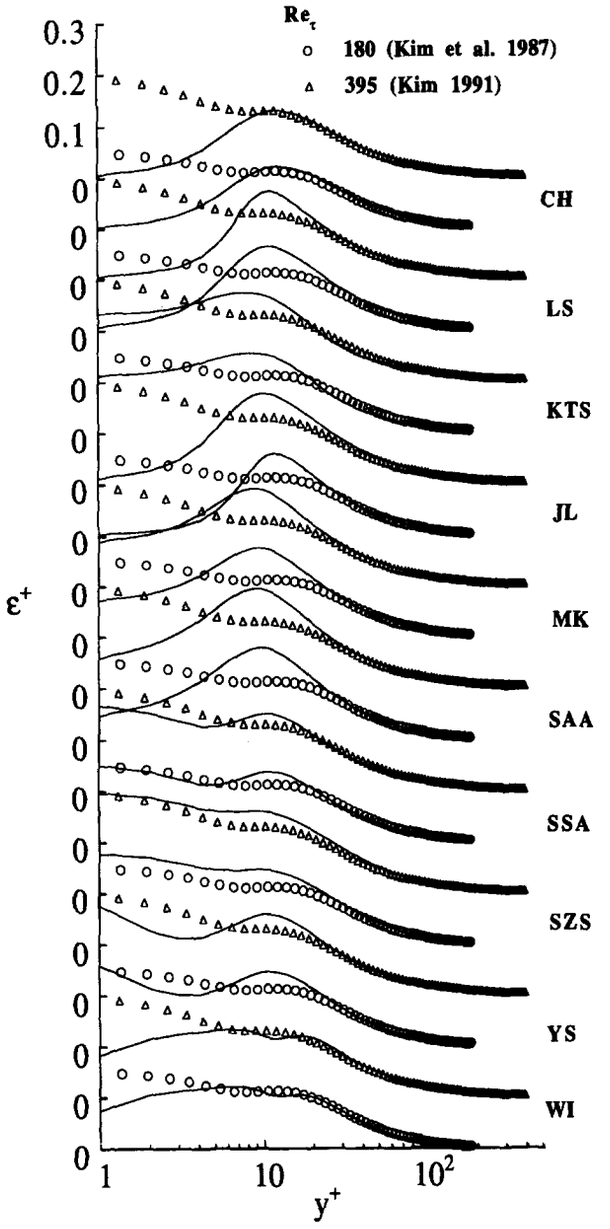

Figure 3 Comparison of calculated ε^+ with data for channel flows

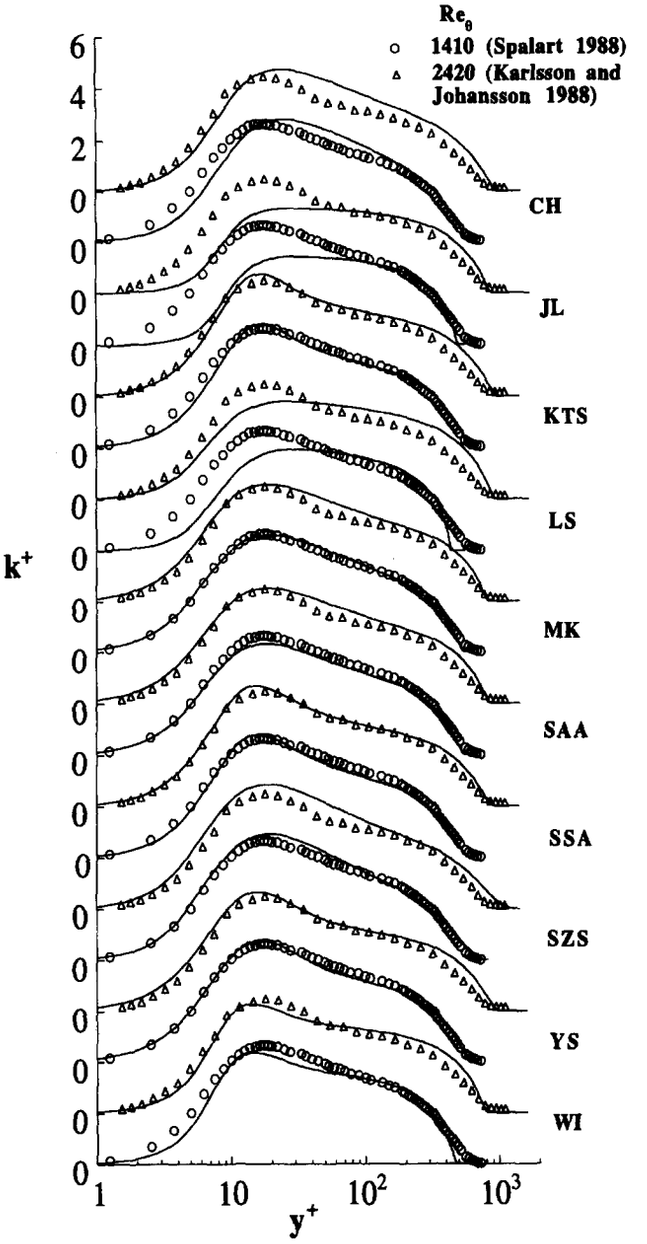

Figure 4 Comparison of calculated k^+ with data for boundary-layer flows

comes in the near-wall region $0 \le y^+ < 25$. Because the ε predicted by the CH, JL, and LS models is a reduced ε, it has to go to zero at the wall, so the comparison in the inner region should be discounted. Although the SAA model does not assume ε to go to zero at the wall, it yields a surprisingly low prediction of ε^+ in the inner region, $0 \le y^+ < 5$, and predicts a maximum away from the wall at about the location where the data indicate a plateau (Figure 3). The performance of WI is, in general, better than SAA and gives a fairly correct prediction of the plateau. As for other k-ε models, the predictions that are in good overall agreement with data for the two Re$_\tau$ cases examined are given by SSA and SZS. On the other hand, YS gives a relatively large variation in the region, $0 \le y^+ < 25$. Among the models investigated, only the SSA, SZS, and YS are capable of predicting a maximum ε^+ at the wall; YS tends to overpredict, while SSA underestimates the maximum slightly (Figure 3). The calculated κ is compared in Table 5. It can be seen that only SSA yields a value of 0.40 ± 0.01 for the two different Re$_\tau$ calculated. All other models give errors larger than this; for CH and KTS, the error is as large as $\pm 25\%$. If the model is asymptotically consistent, then the values of $\varepsilon_w^+/2$ and a_k are identical. It can be seen that four models, MK, SSA, SZS, and YS, satisfy this criterion (Table 5). However, only SSA and SZS yield an a_k that is in reasonable agreement with the DNS data, while YS overpredicts it by more than 60% and MK underestimates by more than 100%. With the exception of LS and WI, the model predictions of a_{uv} are in agreement with DNS data to within the same order (Table 5). Obviously, the prediction of this quantity has little or no effect on the overall calculations of $-uv^+$ and U^+ which are in good agreement with data.

With the exception of KTS, SSA, SZS, and YS, the predictions of U^+ in boundary-layer flows are, in general, poorer compared to those in channel and Couette flows. Again, in these

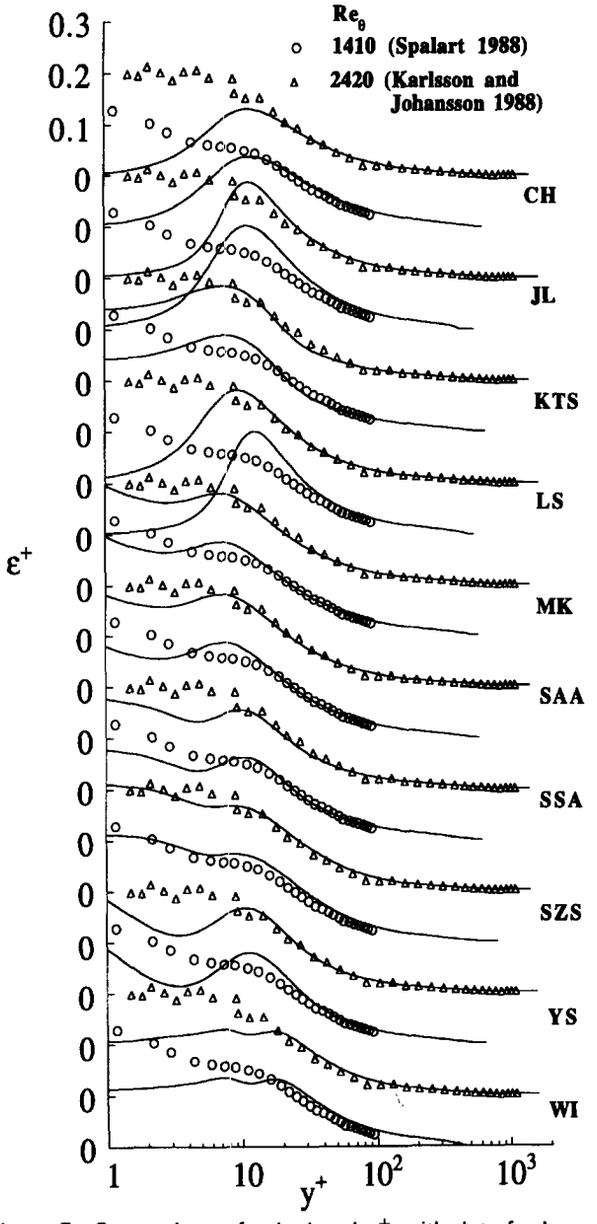

Figure 5 Comparison of calculated ε^+ with data for boundary-layer flows

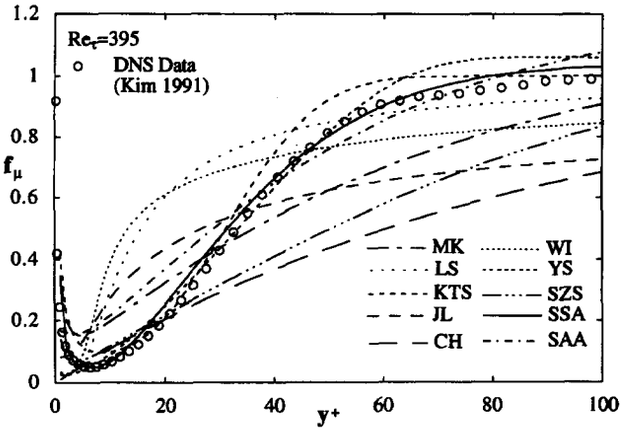

Figure 7 Comparison of calculated f_μ with data for channel flow at $Re_\tau = 395$

models, their performance seems to depend on Re_θ. Some models give a better prediction at a lower Re_θ, such as MK and SAA, while others yield more correct results at higher Re_θ, such as CH and LS. The incorrect predictions can be attributed to errors in the estimate of C_f whose values are compared in Table 6. Overall, the error in the prediction of C_f is within 10% of that given by the data, except those of MK and SAA. The best predictions are rendered by SSA, SZS, and YS, which are correct to within 4%. From Table 6, it is clear that a correct calculation of C_f does not automatically yield an equally correct prediction of κ. The two models that give correct predictions of κ and C_f for the two Reynolds numbers investigated are SSA and YS. This result together with those obtained from Couette and channel flows show that SSA and YS, in general, outperform all other models. The predictions of k^+ by JL and LS are quite poor, because the models fail to reproduce the behavior of the distributions correctly. Other models give a fairly accurate prediction of the behavior of the k^+ distribution across the boundary layer (Figure 4). In particular, KTS, SSA, and YS mimic the k^+ distribution quite well. The characteristics of the calculated ε^+ are similar to the channel flow case (Figure 5). For this flow though, two models, MK and SZS, predict a fairly correct behavior of ε^+ in the region, $1 < y^+ < 10$. However, it should be pointed out that four models, KTS, MK, SAA, and WI, give a maximum ε^+ away from the wall, while SSA, SZS, and YS predict a maximum at the wall. The latter results are more in line

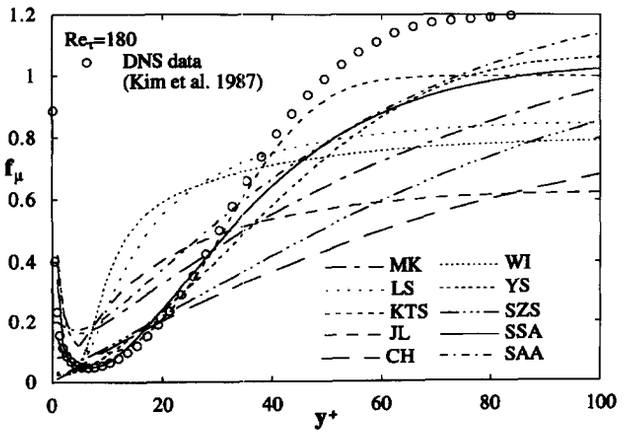

Figure 6 Comparison of calculated f_μ with data for channel flow at $Re_\tau = 180$

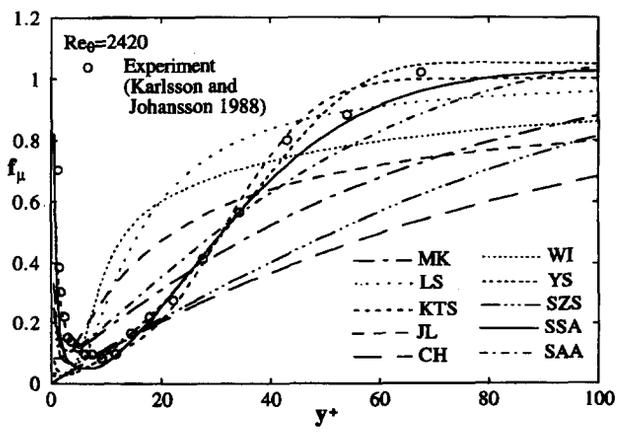

Figure 8 Comparison of calculated f_μ with data for boundary-layer flow at $Re_\theta = 2420$

with DNS and experimental data which show a maximum at the wall. Again, the models KTS, SSA, SZS, and YS give rise to asymptotically consistent results, however, only SSA and SZS yield an a_k that is in fair agreement with data.

Finally, the comparisons of f_μ with DNS channel flow data (Kim et al. 1987; Kim 1991) and boundary-layer measurements (Karlsson and Johansson 1988) are shown in Figures 6–8. It should be noted that f_μ is specifically formulated to match the experimental boundary-layer data in the KTS model (Figure 8); however, its performance for the channel flow case is not as good as that given by SSA and YS (Figure 7) for the $Re_\tau = 395$ case, but it does correlate well with DNS data in the region $0 < y^+ < 50$ for the $Re_\tau = 180$ case (Figure 6). The predictions of SSA and YS are also in agreement with data up to $y^+ = 30$ for the $Re_\tau = 180$ case (Figure 6). It should be noted that f_μ evaluated from DNS data for this case does not go to one away from the wall. This is the reason why the predicted results of KTS, SSA, and YS are not in agreement with data in the outer region. On the other hand, SSA and YS also predict the measured f_μ fairly well in the boundary-layer case (Figure 8). In general, the calculated f_μ of JL, LS, and WI yield curves with very narrow dips, while those of CH, MK, and SZS give very slow rise from the minimum to the asymptotic value. The prediction of SAA is between those of JL, LS, WI and CH, MK, SZS and is rather poor compared to those of KTS, SSA, and YS. These results indicate that whenever the model calculations of U^+, $-\overline{uv}^+$, k^+, and ε^+ are in general agreement with data, the calculated f_μ also correlates well with DNS data and experimental measurements.

Comparisons with backstep flow

Having assessed the performance of the models against simple flows, the next step is to examine their abilities to predict complex flows. A complex flow case where DNS data are available is the backstep flow investigated by Le et al. (1993). An experimental investigation of this same backstep flow has been carried out by Jovic and Driver (1994), and their measurements are also used to validate the model calculations. This flow consists of the following phenomena; separation, recirculation, reattachment, and the development of a boundary layer downstream of the reattachment point. The backstep flow also involves shear-layer mixing in the region bounded by the recirculation and forward flow. Furthermore, the geometry undergoes an expansion, therefore, downstream of the step entrance, the flow experiences an adverse pressure gradient. Therefore, this simple two-dimensional (2-D) flow embodies all the fundamentals of complex flows and is a real test of any two-equation model. The geometry of the backstep flow (Le et al., 1993; Jovic and Driver, 1994) has an expansion ratio of 1.125 and a Reynolds number based on uniform inlet velocity U and step height h of 5100. This set of DNS and experimental data provides by far the most complete measurements of $C_f = 2\tau_w/\rho U^2$ on the step wall and distributions of mean velocity and turbulence statistics up to $20h$. Here, τ_w is the wall shear stress. In view of this, sufficient data are available to assess the models' ability to replicate flow separation, recirculation, reattachment and the subsequent boundary-layer development downstream of the reattachment point.

In this assessment, only five models are considered: CH, LS, MK, SSA, and YS. This choice consists of two of the early models (CH and LS) identified by Patel et al. (1985) as reasonably good, one model (MK) representative of more recent proposals but fails to give overall good results for the simple flows tested, and two recent models (SSA and YS) identified above as performing well against the DNS data of simple flows. All five models are of the k-ε type. Among the five models, the only local model is LS, while others are not. Because the performance of the k-τ and k-ω models are not comparable to those of SSA and YS, the performance of these models is not assessed in this section. The 2-D elliptic code of So et al. (1988) is used to calculate the backstep flow, and the calculation domain extends from the step entrance ($x = 0$) to $x = 50h$. Therefore, the parabolic condition can be assumed at the exit. So et al. (1988) found that a grid of $78(x)$ by $66(y)$ is sufficient to give grid independent solutions for the four Reynolds-stress and one two-equation models considered. Of these five, four are near-wall models. For the present study, the grid is refined to 91 by 81 with 30 grid points concentrated in the region, $0 \le y^+ < 50$. With this grid, all model calculations are found to be grid independent.

The comparison of the calculated C_f with data is shown in Figure 9, while the estimated reattachment length is tabulated in the accompanied table in the figure. With the exception of LS, the other four models yield predictions of the reattachment length correct to within 10%. It is clear that models with explicit y^+ dependence in f_μ (CH and MK) yield an incorrect behavior of C_f in the vicinity of the reattachment point. As a result, their predicted recovery is also in error. The local model (LS) gives the worst C_f distribution, with a large overshoot followed by a sudden drop in the immediate vicinity of the reattachment point. This behavior is indicative of the incorrect prediction by LS of the recirculation and reattachment regions. On the other hand, YS slightly overpredicts, while SSA gives a fairly accurate estimate of the C_f distribution downstream of its minimum. Comparisons of the shear stress, $-\overline{uv}$, and k distributions at $x/h = 4$, 6, 10, 15, and 19 are shown in Figures 10 and 11, respectively. Again, SSA gives fairly accurate predictions of these variables. The next best is given by LS and YS, where they overestimate slightly the maximum value of k (Figure 10). Other model predictions are in error by different amounts. In certain locations, the maximum k is greatly overpredicted (Figure 10), while, in other locations, the $-\overline{uv}$ is vastly underestimated (Figure 11). It seems that incorrect predictions of the C_f distributions by LS and YS have little effects on the calculations of $-\overline{uv}$ and k. Overall, these results tend to show that SSA can replace the behavior of a backstep flow quite well.

Conclusions

Ten near-wall two-equation models of the k-ε, k-τ, and k-ω type are used to calculate simple 2-D flows where detailed DNS and experimental data are available. In particular, the models are

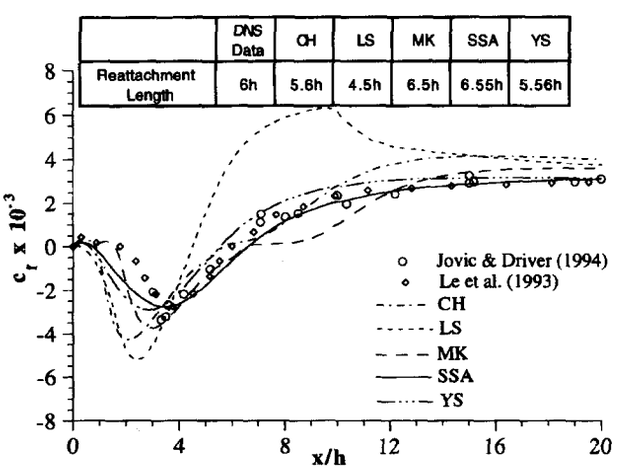

Figure 9 Comparison of calculated C_f with data for backstep flow

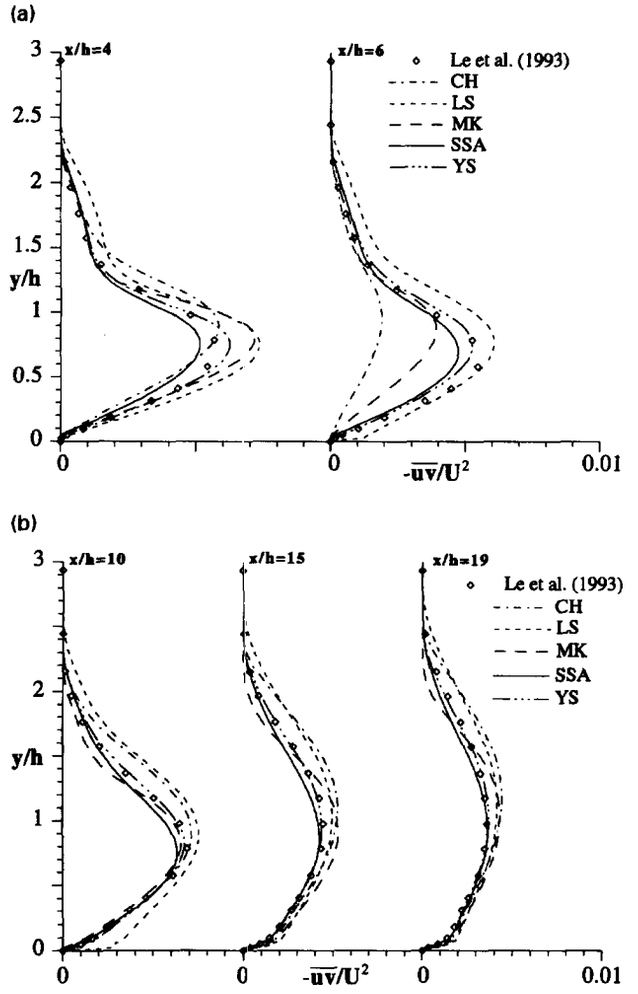

Figure 10 Comparison of calculated shear stress with data for backstep flow

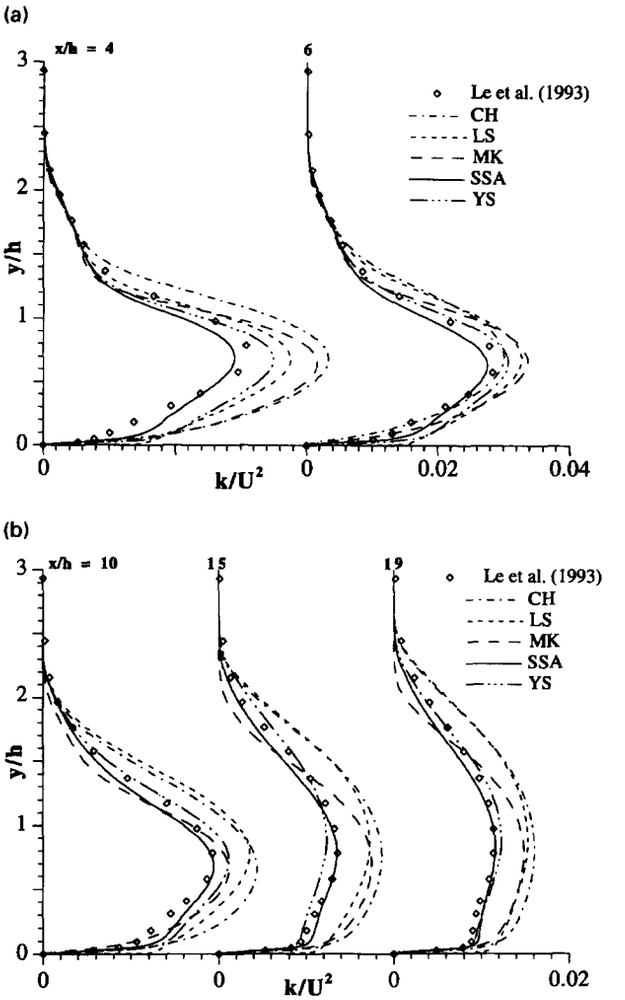

Figure 11 Comparison of calculated k with data for backstep flow

assessed for their ability to calculate Couette flows, where conventional two-equation and second-order models fail to predict the spatial distribution of k^+ correctly. Detailed comparisons with DNS data reveal that an asymptotically consistent near-wall model is important to the correct prediction of turbulent Couette flows. When an asymptotically consistent near-wall model is used, the flow properties near the wall as well as far away from the wall are calculated with fair accuracy. On the other hand, if the near-wall model is not quite asymptotically consistent, the predictions of the mean velocity and turbulent shear stress are still in relatively good agreement with DNS data; however, its predictions of k is incorrect, both in the near-wall region and in the central core of the channel. In general, models whose damping functions are independent of y^+ yield better agreement with data than those that are dependent. For the latter kind of models, the performance is dependent on the flow type as well as the flow Reynolds numbers. Overall, the k-ε models that are asymptotically consistent perform better than the k-ω and k-τ models in the six flow cases considered. Besides, there is no real numerical advantage to solve the k-ω and k-τ models compared to the k-ε models. The boundary conditions invoked for ε poses no real numerical problems as far as numerical stability is concerned. Among the five k-ε models that solve for the true ε, only SSA, SZS, and YS are capable of giving the correct trend for ε in the very near-wall region. However, it seems that the correct prediction of ε in this region has little effect on the calculation of the distributions of other properties away from the wall. It does, however, affect the calculated a_k, ε_w, a_{uv}, u_τ, and κ. This study shows further that another important feature to model correctly is the near-wall behavior of the damping function f_μ. Because SSA and YS are asymptotically consistent and yield a fairly correct calculation for f_μ, their predictions of the three basic simple flows are, in general, better than all other two-equation models examined.

Five of these models, CH, LS, MK, YS, and SSA, are used to calculate a backstep flow where DNS and experimental data are available. All five models examined give a fairly accurate prediction of the reattachment length, correct to within 10%. Furthermore, the results show that models with explicit y^+ dependence in f_μ (CH and MK) yield at C_f distribution that is not very realistic around the reattachment point. On the other hand, LS yields a large overshoot and a sudden drop in C_f in the surrounding region of the reattachment point, while YS slightly overestimates C_f downstream of its minimum. Only SSA gives a fairly correct prediction of the C_f distribution downstream of its minimum point. As for the predictions of the mean velocity, $-\overline{uv}$ and k, the overall best results are given by SSA. In view of this, it can be concluded that SSA is capable of mimicking the complex behavior of a backstep flow fairly well, while other models tested give results that are in error to different degree. These calculations further demonstrate the importance of asymptotic consis-

tency in near-wall modeling as well as having an f_μ that behaves properly in the near-wall region.

Acknowledgments

Research support under Grant PL0008587-AG, Knolls Atomic Power Laboratory, Schenectady, NY 12301 is gratefully acknowledged. The grant was monitored by R. Kunz.

References

Abe, K., Kondoh, T. and Nagano, Y. 1994. A new turbulence model for predicting fluid flow and heat transfer in separating and reattaching flows—I flow field calculations. *Int. J. Heat Mass Transfer*, **37**, 139–151

Alfredsson, P. H., Johansson, A. V., Haritonidis, J. H. and Eckelmann, H. 1988. The fluctuating wall-shear stress and the velocity field in the viscous sublayer. *Phys. Fluids*, **31**, 1026–1033

Chien, K. Y. 1982. Predictions of channel and boundary layer flows with a low-Reynolds-number two-equation model of turbulence. *AIAA J.*, **20**, 33–38

Deng, G. B. and Piquet, J. 1991. k-ε turbulence model for low Reynolds number wall-bounded shear flow. *Proc. 8th Turbulent Shear Flows*, (Paper 26-2), Technical University of Munich, Munich, Germany

Durbin, P. A. 1991. Near-wall turbulence models without damping functions. *Theoret. Comp. Fluid Dynamics*, **3**, 1–13

Hanjalic, K. 1994. Advanced turbulence closure models: A view of current status and future propects. *Int. J. Heat Fluid Flow*, **15**, 178–203.

Henry, F. S. and Reynolds, A. J. 1984. Analytical solution of two gradient-diffusion models applied to turbulent Couette flow. *J. Fluids Eng.*, **106**, 211–216.

Jones, W. P. and Launder, B. E. 1972. The prediction of laminarization with two-equation model of turbulence. *Int. J. Heat Mass Transfer*, **15**, 301–314

Jovic, S. and Driver, D. 1994. Backward-facing step measurements at low Reynolds number. NASA TM-108870

Karlsson, R. I. and Johansson, T. G. 1988. LDV measurements of higher order moments of velocity fluctuations in a turbulent boundary layer. In *Laser Anemometry in Fluid Mechanics*, D. F. G. Durao et al. (eds.), Portugal, Ladoan-Instituto Superior Tecnico, 273–289.

Karlsson, R. I., Tinoco, H. and Svenson, U. 1991. An improved form of the near-wall k-ε model based on new experimental data. *Proc. 8th Turbulent Shear Flows*, (Paper 26-3), Technical University of Munich, Munich, Germany

Kim, J., Moin, P. and Moser, R. D. 1987. Turbulence statistics in fully developed channel flow at low Reynolds Number. *J. Fluid Mech.*, **177**, 133–186

Kim, J. 1991. Private communication

Kristoffersen, R., Bech, K. H. and Andersson, H. I. 1993. Numerical study of turbulent plane Couette flow at low Reynolds number. *Appl. Sci. Research*, **51**, 337–343

Launder, B. E. and Sharma, B. I. 1974. Application of the energy dissipation model of turbulence to the calculation of flow near a spinning disc. *Lett. Heat Mass Transfer*, **1**, 131–138

Launder, B. E. 1986. Low-Reynolds-number turbulence near walls. Rept. TFD/86/4, Mechanical Engineering Department UMIST, Manchester, UK

Le, H., Moin, P. and Kim, J. 1993. Direct numerical simulation of turbulent flow over a backward-facing step. Rept. TF-58, Thermosciences Division, Mechanical Engineering Department, Stanford University

Lee, M. J. and Kim, J. 1991. The structure of turbulence in a simulated plane Couette flow. *Proc. 8th Turbulent Shear Flows*, (Paper 5-3), Technical University of Munich, Munich, Germany

Mansour, N. N. and Shih, T. H. 1989. Advancement in turbulence modeling. In *Forum on Turbulent Flows*—1898, W. W. Bower and M. J. Morris, (eds.), FED-76, 129–141.

Mansour, N. N., Kim, J. and Moin, P. 1988. Reynolds-stress and dissipation-rate budgets in a turbulent channel flow. *J. Fluid Mech.*, **194**, 15–44.

Michelassi, V., Rodi, W. and Scheuerer, G. 1991. Testing a low Reynolds number k-ε turbulence model based on direct simulation data. *Proc. 8th Turbulent Shear Flows*, (Paper 26-5), Technical University of Munich, Munich, Germany

Moser, R. D. and Moin, P. 1987. The effects of curvature in wall-bounded turbulent flows. *J. Fluid Mech.*, **175**, 479–510

Myong, H. K. and Kasagi, N. 1990. A new approach to the improvement of the k-ε turbulence model for wall bounded shear flows. *JSME Int. J.*, **33**, 63–72

Nagano, Y. and Hishida, M. 1987. Improved form of the k-ε model for wall turbulent shear flows. *J. Fluids Eng.*, **109**, 156–160

Nagano, Y. and Tagawa, M. 1990. An improved k-ε model for boundary layer flows. *J. Fluids Eng.*, **112**, 33–39

Nishino, K. and Kasagi, N. 1989. Turbulence statistics measurement in a two-dimensional channel flow using a three-dimensional particle tracking velocimeter. *Proc. 7th Symposium on Turbulent Shear Flows*, (Paper 22-1), Stanford University, Stanford, CA.

Nisizima, S. and Yoshizawa, A. 1987. Turbulent channel and Couette flows using an anisotropic k-ε model. *AIAA J.*, **25**, 414–420

Patel, V. C., Rodi, W. and Scheuerer, G. 1985. Turbulence models for near-wall and low-Reynolds-number flows: A review. *AIAA J.*, **23**, 1308–1319

Rodi, W. and Mansour, N. N. 1993. Low Reynolds number k-ε modeling with the aid of direct simulation data. *J. Fluid Mech.*, **250**, 509–524

Sarkar, A. 1995. An improved near-wall k-ε model for the calculation of wall-bounded turbulent flows. Master's thesis, Mechanical and Aerospace Engineering, Arizona State University, Tempe, AZ

Schneider, W. 1989. On Reynolds stress transport in turbulent Couette flow. *Z. Flugwiss. Weltraumforsch.*, **13**, 315–319

So, R. M. C., Lai, Y. G., Hwang, B. C. and Yoo, G. J. 1988. Low-Reynolds-number modeling of flows over a backward-facing step. *ZAMP*, **39**, 13–27

So, R. M. C., Lai, Y. G., Zhang, H. S. and Hwang, B. C. 1991a. Second-order near-wall turbulence closures: A review. *AIAA J.*, **29**, 1819–1835

So, R. M. C., Zhang, H. S. and Speziale, C. G. 1991b. Near-wall modeling of the dissipation-rate equation. *AIAA J.*, **29**, 2069–2076

So, R. M. C., Aksoy, H., Yuan, S. P. and Sommer, T. P. 1994. Development of a near-wall Reynolds-stress closure based on the SSG model for the pressure strain. NASA Contractor Rept. 4618

Spalart, P. R. 1988. Direct simulation of a turbulent boundary layer up to $R_\theta = 1410$. *J. Fluid Mech.*, **187**, 61–98

Speziale, C. G., Abid, R. and Anderson, E. C. 1990. A Critical evaluation of two-equation models for near wall turbulence. AIAA Paper 90-1481

Wilcox, D. C. 1994. Simulations of transition with a two-equation turbulence model. *AIAA J.*, **32**, 247–255

Yang, Z. and Shih, T. H. 1993. New time scale based k-ε model for near-wall turbulence. *AIAA J.*, **31**, 1191–1198

Zhang, H. S., So, R. M. C., Speziale, C. G. and Lai, Y. G. 1993. A near-wall two-equation model for compressible turbulent flows. *AIAA J.*, **31**, 196–199